Kinetics of a one-dimensional granular medium in the quasielastic limit

Sean McNamara and W. R. Young
Scripps Institution of Oceanography, La Jolla, California 92093-0230

The dynamics of a one-dimensional granular medium has a finite time singularity if the number of particles in the medium is greater than a certain critical value. The singularity ("inelastic collapse") occurs when a group of particles collides infinitely often in a finite time so that the separations and relative velocities vanish. To avoid the finite time singularity, a double limit in which the coefficient of restitution r approaches 1 and the number of particles N becomes large, but is always below the critical number needed to trigger collapse, is considered. Specifically, $r \to 1$ with $N \sim (1-r)^{-1}$. This procedure is called the "quasielastic" limit. Using a combination of direct simulation and kinetic theory, it is shown that a bimodal velocity distribution develops from random initial conditions. The bimodal distribution is the basis for a "two-stream" continuum model in which each stream represents one of the velocity modes. This two-stream model qualitatively explains some of the unusual phenomena seen in the simulations, such as the growth of large-scale instabilities in a medium that is excited with statistically homogeneous initial conditions. These instabilities can be either direct or oscillatory, depending on the domain size, and their finite-amplitude development results in the formation of clusters of particles.

I. INTRODUCTION

The one-dimensional granular medium has been studied recently by us[1] and by others.[2] The model is an ensemble of inelastic point particles, all with the same mass, moving on a line. In this model, the collisions conserve momentum but dissipate kinetic energy. Thus the velocities after a collision, u'_1 and u'_2, are related to the velocities before collision, u_1 and u_2, by

$$u'_1 = \tfrac{1}{2}(1-r)u_1 + \tfrac{1}{2}(1+r)u_2,$$
$$u'_2 = \tfrac{1}{2}(1+r)u_1 + \tfrac{1}{2}(1-r)u_2. \tag{1}$$

Here, $0 \leqslant r \leqslant 1$ is the coefficient of restitution, i.e., $u'_1 - u'_2 = -r(u_1 - u_2)$. If $r = 1$, the collisions are perfectly elastic and the system is the classical, one-dimensional perfect gas. If $r = 0$, the collisions are perfectly inelastic and the system studied in Ref. 3 is recovered. In between these two extremes, the system is a simple model of a one-dimensional "granular medium."

With this idealized one-dimensional model, we can isolate and understand some of the physics peculiar to granular flows. For example, studies of two-dimensional granular chute flows[4] and shear flows[5] have found a tendency for particles to form clusters surrounded by low-density regions. The simulations show that this clumping is more severe for more inelastic particles. In Ref. 5 these clumps and voids are referred to as "inelastic microstructure." Now, in one-dimensional granular mechanics, particles can collide infinitely often in finite time[1,2] so that both the relative velocities and separations of the particles vanish. This finite time singularity, referred to in Ref. 1 as "inelastic collapse," results in the formation of one-dimensional clumps and voids. It is a plausible speculation that the formation of inelastic microstructure in two-dimensional simulations is related to one-dimensional inelastic collapse. But the connection is not conclusive because it has not

been demonstrated that two-dimensional inelastic particles can collide infinitely often in finite time. The advantage of the one-dimensional case is that analytic results are available [e.g., Eqs. (2) and (3) below] and that theoretical assumptions and approximations can be examined with simple simulations.

Hydrodynamic models of granular flows[6,7] offer an analytic avenue into the issue of microstructure formation. Reference 8 uses linear hydrodynamic stabilty theory to explain clustering as an instabilty of a granular flow with uniform density.[9] One very significant result[8] is that the instability is confined to long wavelengths. Consequently, numerical simulations in small periodic domains will be stable because the quantization condition on the long unstable waves cannot be satisfied. If the particle density is fixed, this condition on the domain size is equivalent to saying that instability requires a minimum number of particles in the domain. Stated in these terms, the criterion for instability in Ref. 8 is similar to the condition for inelastic collapse in Refs. 1 and 2. There, it is shown that, for a given value of the coefficient of restitution r, there is a minimum number of particles $N_{\min}(r)$ required for inelastic collapse.

The "independent collision wave" (ICW) approximation,[2] estimates this relation between $N_{\min}$ and r as

$$r = \tan^2[(\pi/4)(1 - 1/N_{\min})]. \tag{2}$$

The numerical results of Ref. 1 showed that Eq. (2) is an accurate estimate of $N_{\min}(r)$ for $r \leqslant 0.8$ (and the ICW approximation is exact as $r \to 0$). An estimate of $N_{\min}(r)$ in the complementary limit $r \to 1$ leads to[1]

$$N_{\min} = \frac{\ln(2/q)}{2q}, \tag{3}$$

where we have used the notation

$$q \equiv \tfrac{1}{2}(1-r). \tag{4}$$

Equation (3) is accurate for $r \gtrsim 0.8$. The two results agree approximately at $r = 0.8$ where numerical simulation shows $N_{\min} = 16$. [The results in Eqs. (2) and (3) give the minimum number of particles required for collapse against an inelastic wall. By symmetry, the minimum number in the middle of the inelastic gas is twice the values in Eqs. (2) and (3).]

Difficulties arise in the kinetic theory of a one-dimensional granular material because of inelastic collapse. Specifically, neighboring particle velocities become correlated and density fluctuations render the continuum assumption invalid. (For the same reasons, kinetic theory fails in higher dimensions once inelastic microstructure develops.) In this paper, we postpone the inevitable formation of particle clusters by investigating the one-dimensional granular medium in the "quasielastic limit." We assume that $r \to 1$ ($q \to 0$) and $N \to \infty$, but require that this double limit satisfies $N < N_{\min}(r)$ so that inelastic collapse does not occur. [For instance, we could take $N \sim 1/(1-r)$ as $r \to 1$.] The number of particles is large and clusters form slowly, so it is possible to use continuum models for a time.

The focus of this work is the cooling of a one-dimensional granular medium in the quasielastic limit. Simulations are used to suggest theoretical approaches. In our simulations, the gas is randomly excited by picking the velocities using a random number generator following which there is no input of energy. As was predicted theoretically,[7] the mean kinetic energy of a particle (also called the granular temperature) then decreases like t^{-2}. In Sec. II, we use numerical simulation to show that the velocity distribution during this t^{-2} cooling process is bimodal; roughly, there is a stream of left-moving particles and a separate stream of right-moving particles. The kinetic theory developed in Secs. III and IV explains this unusual distribution of velocities.

The Maxwellian velocity distribution of an ideal gas is not expected in the one-dimensional granular medium, because it requires at least two dimensions to arise. In two or three dimensions, a collision between two perfectly elastic particles can have many different outcomes which conserve both energy and momentum. Thus, the velocity distribution of the gas can change with time because the particles can scatter each other into a number of different directions. However, if perfectly elastic particles are constrained to move in one dimension, then collisions simply exchange velocities, so the velocity distribution never changes. The one-dimensional, bimodal velocity distribution arises solely because the collisions are slightly inelastic. In two- and three-dimensional granular flows, these effects compete with the multidimensionality of the space.

The simulations also show that clumping of particles occurs even when $N < N_{\min}(r)$. This clumping is not as severe as that associated with inelastic collapse. For instance, the collision count remains finite and the interparticle spacing is nonzero (but very unevenly distributed). But position and velocity correlations do develop as the gas
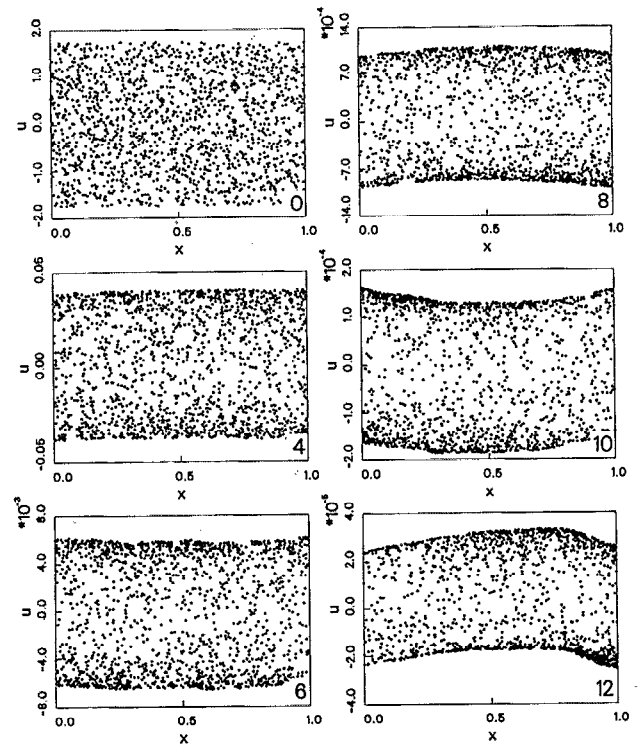

FIG. 1. Cooling of a one-dimensional granular media with $L=2$ ($r=0.998\,75$, $N=1600$). Each dot marks the location of a particle in (x,u) space. As the gas cools, the velocity scales contract. Each panel is a "snapshot" of the cooling at a particular value of $\tau_c \equiv 2LN_c/N^2$, given in the lower right-hand corner of each panel. The first panel, marked with a 0 is the initial condition. The particles are uniformly distributed between $u = \pm\sqrt{3}$ to give $U^2 \approx 1$ [U^2 is defined in Eq. (8)]. Each unit of τ_c is 6.4×10^5 collisions.

cools in the quasielastic limit. The kinetic theory developed of Secs. III and IV is directed toward the initial development of velocity and position correlations, but begins to fail once these correlations become strong. The theory appears to be equally valid for the quasielastic limit and for the initial stages of inelastic collapse, provided $N_{\min} \gg 1$.

Finally, we emphasize that the focus of this article is confined to an unforced medium in which the kinetic energy present in the initial condition is dissipated without replenishment. Other simulations and experiments consider forced flows in which kinetic energy is continually supplied by either shearing the boundaries of the medium[5] or by the release of gravitational potential energy.[4,10]

II. NUMERICAL SIMULATIONS

Figures 1–3 show the phase space of simulations of the cooling, one-dimensional granular medium. Figures 1 and 2 show the same simulation at different stages in its evolution while Fig. 3 shows a second simulation with a smaller coefficient of restitution. The initial conditions for both simulations are the same and are shown in the first panel of Fig. 1. The positions of 1600 particles are uniformly distributed between the two inelastic walls at $x=0$ and 1. The velocities are uniformly distributed in the interval $-\sqrt{3} < u < \sqrt{3}$. As the simulation evolves, the parti-
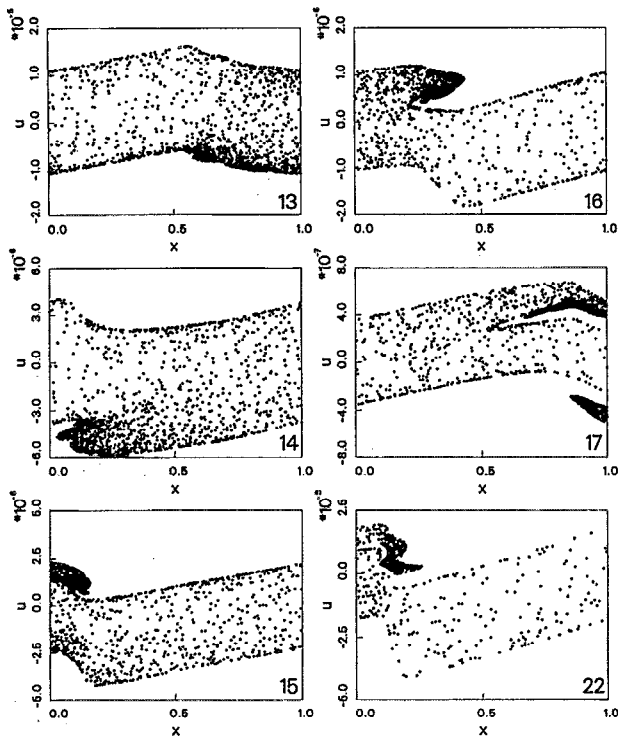
    S. McNamara and W. R. Young

FIG. 2. The same experiment as in Fig. 1, except at a later stage in its development. The numbers give the value of τ_c for each panel. At $\tau_c = 14$, the large clump in the lower left-hand corner is about to collide with the wall at $x = 0$. After $\tau_c = 17$, the clump travels across the domain to the wall at $x = 0$, and bounces off that wall. At $\tau_c = 22$, most of the particles are concentrated in the crescent-shaped clump near $x = 0.1$. The top of the crescent is moving faster than the bottom, so the crescent is soon stretched out into a diagonal line.

cles dissipate kinetic energy through collisions and no further energy is added. Thus the velocities decrease with time, and the velocities scales on each panel of the figure are different. Our discussion of these figures will anticipate

FIG. 3. Cooling of a one-dimensional granular media with $L = 8$ ($r = 0.995$, $N = 1600$). Each dot marks the location of a particle in (x,u) space. The numbers give the value of τ_c for each panel. (Each unit of τ_c is 1.6×10^5 collisions.)

some results from the kinetic theory of Secs. III and IV. Specifically, we characterize each simulation with the quantity

$$L \equiv 2qN, \qquad (5)$$

where q is a measure the coefficient of restitution, defined in Eq. (4), and N is the number of particles in the simulation.

We measure time with a "collision time" defined to be

$$\tau_c \equiv 2L(N_c/N^2), \qquad (6)$$

where N_c is the cumulative number of collisions since the beginning of the simulation. Each collision corresponds to a "tick" of the collision clock; as the medium cools, collisions occur less frequently, and the clock runs more slowly. The quantity τ_c measures the amount of time that has elapsed on the clock. Both L and τ_c will reappear in the theory presented in the later sections.

All three figures show the emergence and persistence of a bimodal velocity distribution. As the gas cools, the particles cluster into two "streams" at the outer edges of the distribution. Particles do not migrate from the center of the distribution toward the edge; rather the distribution is continuously contracting, with particles at the edges moving more quickly toward the center than those near the middle. Thus the two modes at the edges form as additional particles are "scooped" up by the contracting bands. In Sec. III, we develop a theory that explains this velocity distribution.

Figure 1 shows a simulation with $L = 2$ and $N = 1600$. Equations (4) and (5) show that these values of N and L require $r = 0.99875$; i.e., almost perfectly elastic particles. [The simulation does not contain enough particles to cause inelastic collapse; Eq. (3) predicts 6457 particles would be required.] Once the bimodal velocity distribution emerges, the streams arch up and then down together. The later panels of Fig. 1 show a coherent vibration of particle density. The amplitude of the vibrations, relative to the width of the band, increases with time. This unstable vibration is subject to nonlinear steepening. When the band arcs upward in phase space, as at $\tau_c = 12$, the particles at the top of the arch are moving in the positive direction (to the right), causing the arch to steepen toward the right. Also, density inhomogenities develop spontaneously. The initial condition has uniform density, but in the last panel, there is a large, growing concentration of particles in the lower right-hand corner. This cluster of particles plays a dominant role in the future evolution of this simulation.

Figure 2 shows the same simulation as Fig. 1, except at later times. In the last panel of Fig. 1, there is an increased concentration of particles in the lower right-hand corner. As the simulation evolves, this clump becomes tighter, and draws in more particles. This clump is not the result of inelastic collapse; it bounces back and forth between the walls indefinitely. Between $\tau_c = 14$ and $\tau_c = 15$ the clump has bounced off the wall at $x = 0$. At $\tau_c = 17$, it is bouncing off the wall at $x = 1$, and at $\tau_c = 22$ it is on its way toward another bounce at $x = 1$. The theory developed later in the paper does not explain the behavior of the particle
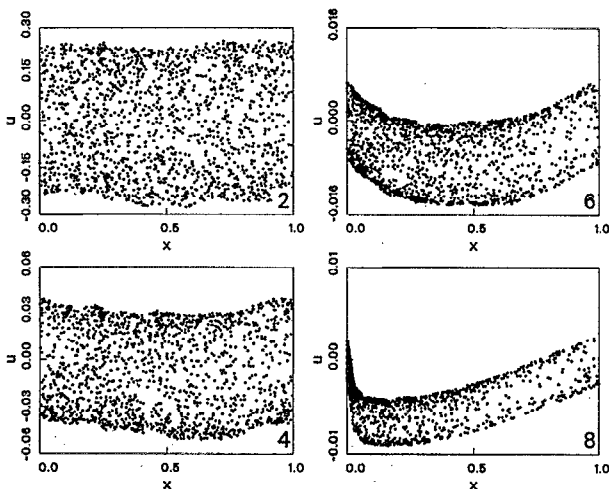
S. McNamara and W. R. Young   36

clumps in Fig. 2 because strong velocity and position correlations invalidate the statistical approach. But the theory does qualitatively explain the initial development of the inhomogeneities in Fig. 1.

All simulations with $L=2$ resulted in large particle clusters similar to the one illustrated in Fig. 2. These clusters form in one of two alternative ways. First, there is the large-scale collective particle motion illustrated in Fig. 1. Alternatively, weak, smaller-scale disturbances form throughout the medium, and grow through merger, but this also leads to situations resembling the later panels of Fig. 2. The difference between the two routes depends on initial conditions (we used a random number generator) which we have not been able to adequately characterize.

Figure 3 shows a less elastic simulation with $L=8$, $N=1600$ (i.e., $r=0.995$). As with the previous simulation, the bimodal velocity distribution emerges and the band of particles begins to bend. The band does not oscillate; rather it grows and nonlinearly steepens. This compresses the particles against the wall at $x=0$. In this case, inelastic collapse will occur; Eq. (3) shows that only 1337 particles are required for inelastic collapse against a wall. Most of the particles at $\tau_c=8$ have $u<0$ and so they are traveling toward the dense particle clump near $x=0$. There are some particles with $u>0$. However, those near $x=0$ are trapped under a larger number of particles heading for the wall. Those near $x=1$ will soon bounce off that wall and begin their journey toward the singularity at $x=0$. Indeed, further simulation suggests that the collision count becomes infinite in a finite time and that the clump near $x=0$ contracts indefinitely.

At $L=8$, the emergence of a growing, stationary wave with a wavelength of twice the domain size occurs in most simulations. (An alternate behavior, exhibited by only one simulation, is shown in Fig. 11, and will be discussed later in this paper.) The wave arches either up or down. This symmetry breaking is caused by differences in the initial conditions. As L is increased (r is decreased), higher harmonics occur. This is illustrated in Fig. 4, where two additional simulations with large L are shown. The relative strengths of these higher wave numbers vary from simulation to simulation.

In Fig. 1, 3, and 4, particles are found in a sharply defined band in phase space, with a nearly constant width. We define the "sinuousity" ξ to be the ratio between the excursions of the band's center to its width. The sinuousity is calculated by dividing the interval $0<x<1$ into ten bins of length $\Delta x=1/10$. Within each bin, the particles with the maximum and minimum (most negative) velocities are located. The difference between these two velocities is taken to be the width of the band, ΔU_i, where $i=1,2,...,10$ is the bin number. The average of these two velocities defines the midpoint of the band $\bar{U}_i$. The amplitude of the band's excursions is defined as the difference between the largest and smallest $\bar{U}_i$. The width of the band is defined by averaging all the ΔU_i. Thus the sinuousity ξ, which is the ratio of these two numbers, is

$$\xi \equiv [\max(\bar{U}_i) - \min(\bar{U}_i)]/\text{mean}(\Delta U_i). \qquad (7)$$
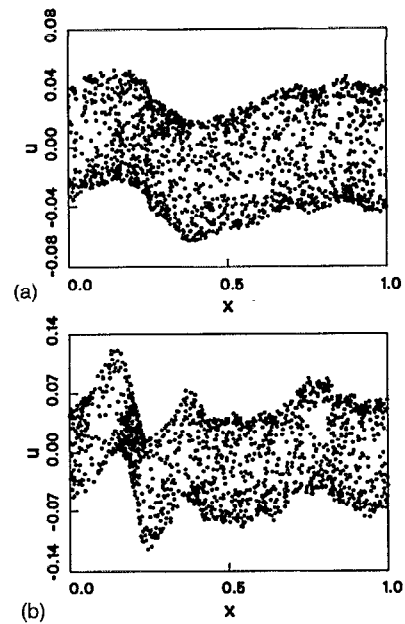

FIG. 4. Two simulations with large L, showing the appearance of shorter length scales relative to the domain size as L increases. Note that the velocity scales are different in the two panels. (a) $L=16$ ($N=1600$, $r=0.99$). (b) $L=32$ ($N=1600$, $r=0.98$). In both figures the sinuousity ξ, defined in Eq. (8), is 0.4.

Figure 5 shows the sinuousity as a function of time for five different simulations, including those shown in Figs. 1–4. All simulations have 1600 particles. The growing and oscillating wave of Fig. 1 appears in Fig. 5 as an oscillation in ξ, superimposed on a steady growth. The stationary,
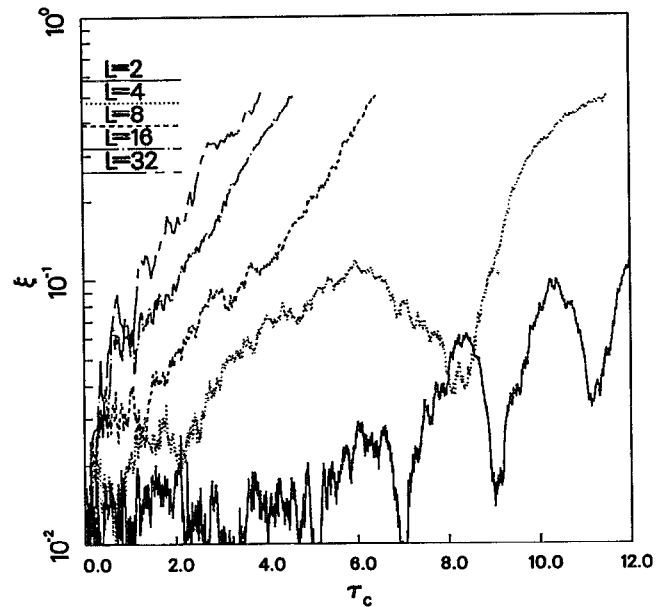

FIG. 5. The sinuousity as a function of time for five simulations. All simulations have 1600 particles. Time is measured by τ_c, as it is in Figs. 1–4. The curves with $L=16$ and $L=32$ are the simulations of Fig. 4. The $L=8$ curve is the simulation in Fig. 3. Figures 1 and 2 show the $L=2$ simulation.
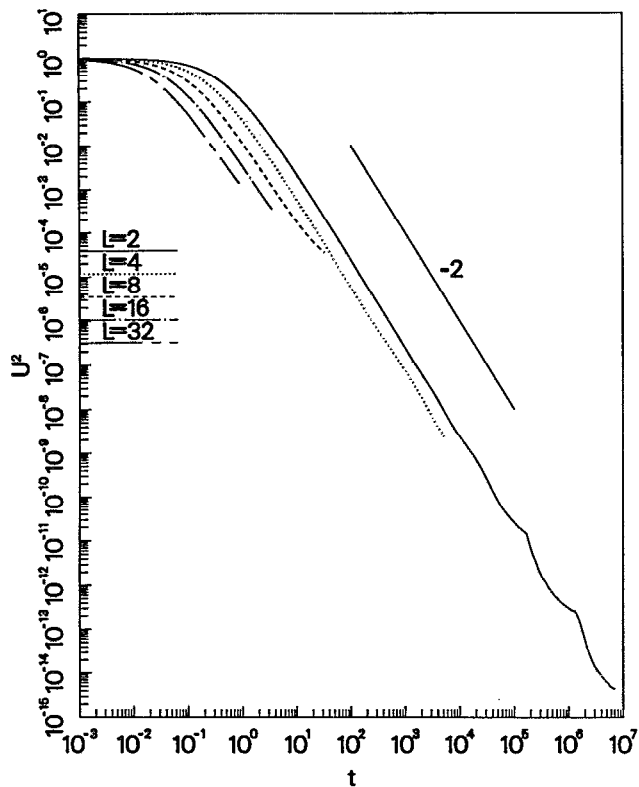
FIG. 6. The granular temperature U^2 versus time for the five simulations of Fig. 5. A line of slope -2 is shown to demonstrate the t^{-2} cooling law. The simulations were stopped when the sinuousity ξ reached 0.5. The "scallops" toward the end of the $L=2$ curve are a result of a large number of particles traveling together in a clump. When a clump hits the wall, the rate of cooling is increased, as the particles in the clump collide with one another. When the clump is traveling in the middle of the domain, the rate of cooling is slower, since there are mainly collisions between the particles in the clump and the sparse background. In all cases, the theoretical result in Eq. (34) is indistinguishable from the simulations until the final stages when the simulations have fluctuations such as the scallops in the $L=2$ curve.

growing wave of Fig. 3 appears as a roughly monotonic increase in ξ. The kinetic theory presented later in this paper predicts growing, traveling disturbances for $L < 2\pi$, and stationary growing disturbances for $L > 2\pi$.

The "granular temperature," U^2, is shown in Fig. 6 as a function of time for the five simulations of Fig. 5. The granular temperature is defined here as

$$U^2 \equiv \frac{1}{N} \sum_{i=1}^{N} u_i^2, \tag{8}$$

where u_i is the velocity of the ith ball relative to the walls at $x=0$ and $x=1$. The granular temperature is proportional to the average kinetic energy per particle. Despite all the drama in Figs. 1–4, the temperature is simply related to t. After a short transient region, the temperature decays at t^{-2}, as predicted by theory in Ref. 7. In Sec. IV, we use a simple model that not only predicts t^{-2} cooling, but can also predict the transient region.

III. PHASE-SPACE DESCRIPTION

In this section, we develop a continuum approximation for the one-dimensional granular medium. Our goal is to understand the phenomenology described in Sec. II. We introduce the phase-space density function $f(u,x,t)$, defining $f(u,x,t)dx\,du$ to be the number of particles located between x and $x+dx$ with velocities between u and $u+du$ at time t. In our model, the two particles involved in a collision are destroyed; instantaneously, two new particles with different velocities are created. The governing equation for f is a one-dimensional Boltzmann equation:[11]

$$f_t + u f_x = C(u,x,t) - A(u,x,t), \tag{9}$$

where $C(u,x,t)$ is the rate of creation of particles with velocity u at position x at time t; $A(u,x,t)$ is their rate of annihilation. Here, $A(u,x,t)$ is the collision rate for a particle of velocity u times the density of particles at that velocity:

$$A(u,x,t) = f(u,x,t) \int |u' - u| f(u',x,t) du'. \tag{10}$$

The creation rate is the collision rate between particles of speeds u' and u'', constrained by Eqs. (1) so that a particle of speed u is created:

$$C(u,x,t) = \int \int |u' - u''| f(u',x,t) f(u'',x,t)$$
$$\times \delta[u - qu' - (1-q)u''] du'\,du'', \tag{11}$$

where q is defined in Eq. (4). In deriving expressions for $A(u)$ and $C(u)$, we assume that the probability of a collision between two particles with velocities u and u' involves only the product $f(u)f(u')$, i.e., the velocities of the two particles are both independent realizations of the same underlying probability distribution. This is the "molecular chaos assumption."

Without the quasielastic limit, the molecular chaos assumption must be invalid because of the strong velocity correlations associated with inelastic collapse. It is ironic that Boltzmann's introduction of this assumption was criticized because of the underlying reversibility of perfectly elastic dynamics. In the present case, it is when the underlying dynamics is most irreversible that the molecular chaos assumption seems most dubious.

A. SIMPLIFICATION OF THE BOLTZMANN EQUATION IN THE ELASTIC LIMIT

We now approximate the δ function in the creation rate, Eq. (11), with a Taylor series, using q as our small parameter:

$$\delta[u - qu' - (1-q)u''] = \delta[u - u'' + q(u'' - u')]$$
$$\approx \delta(u - u'') + q(u'' - u')\delta'(u - u'')$$
$$+ \tfrac{1}{2}q^2(u'' - u')^2 \delta''(u - u'')$$
$$+ \cdots, \tag{12}$$

where the primes on the δ's indicate differentiation. Putting this into our expression for the creation rate, and integrating over u'', we have

$$C(u,x,t) = f(u,x,t) \int |u'-u| f(u',x,t) du'$$

$$+ \partial_u \left(q f(u,x,t) \int |u'-u| (u-u') \right.$$

$$\left. \times f(u',x,t) du' \right) + \partial_u^2 \left(\frac{1}{2} q^2 f(u,x,t) \int |u'-u| \right.$$

$$\left. \times (u-u')^2 f(u',x,t) du' \right) + O(q^3). \qquad (13)$$

Defining an acceleration

$$a(u,x,t) \equiv q \int |u'-u| (u'-u) f(u',x,t) du', \qquad (14)$$

and a diffusivity

$$D(u,x,t) \equiv \frac{1}{2} q^2 \int |u'-u| (u'-u)^2 f(u',x,t) du', \qquad (15)$$

we can write the creation rate as

$$C(u,x,t) = A(u,x,t) - (af)_u + (Df)_{uu}, \qquad (16)$$

where terms of order q^3 have been neglected. The Boltzmann equation then takes the form

$$f_t + u f_x + (af)_u = (Df)_{uu} + O(q^3). \qquad (17)$$

B. The test-particle equation

Retaining terms in Eq. (17) up to $O(q)$ only, we arrive at the "test-particle equation,"

$$f_t + (uf)_x + (af)_u = 0, \qquad (18)$$

where $a(x,u,t)$ is given in Eq. (14). This is the most brutal truncation of the expansion in Eqs. (12) and (13) that still retains the effects of inelasticity. Because the remainder of this paper uses Eq. (18), a less formal and more physical derivation of it is instructive.

We begin by considering Eq. (18) as a continuity equation in phase space, expressing conservation of particles. Since u is a coordinate, all that remains is to calculate the acceleration, $a(x,u,t) = \dot{u}$. In the limit of $r \to 1$, it can be seen from the collision rule, Eq. (1), that two particles colliding very nearly exchange velocities. Thus the accelerations are large; the particles continually rattle back and forth between their neighbors. However, $(af)_u$ is proportional to q, and should vanish as $r \to 1$. This paradox is resolved by exchanging the identities of the particles during collisions. Particles then pass through each other perturbing each other's velocity by an amount of order qU.

We assume that the acceleration a particle experiences depends only on its velocity u and position x. We imagine one particle, called the "test particle," moving at velocity u

through the swarm of nearly elastic particles. We suppose that the mean acceleration of this test particle characterizes the acceleration of *all* of the particles with velocity u.[12] Each collision modifies the test particle's velocity slightly. We can define an acceleration at a point x which is the integrated effect of many, finite, discrete collisions within a neighborhood dx of x. Calculating this acceleration, we consider a collision between our test particle and another particle moving at velocity u'. The collision modifies the test-particle velocity by the amount

$$\Delta u / \text{collision} = q(u'-u). \qquad (19)$$

The test particle encounters particles with speeds between u' and $u' + du'$ at the rate of

$$\text{collisions}/\Delta t = |u'-u| f(u') du'. \qquad (20)$$

The acceleration due to these particles is

$$da = \Delta u / \Delta t = q(u'-u) |u'-u| f(u') du'. \qquad (21)$$

Integrating over u' gives Eq. (14) for the acceleration of the test particle.

If the test particle has a velocity much larger than any neighboring particles, the acceleration is $a = -q\rho u^2$, quadratic in u. One factor of u arises because the collision rate is proportional to u; the other occurs because each collision perturbs the velocity by an amount proportional to u. In the other limit, $u \to 0$, if f is symmetric about $u=0$, a is proportional to u: $a = -2qu \int |u'| f(u') du'$.

C. Some properties of the test-particle equation

In this section, we derive continuity, momentum, and energy equations, and show that particles and momentum are conserved and that energy is dissipated. In addition, we show that the test-particle equation is Galilean invariant.

The density ρ, macroscopic velocity v, and the granular temperature θ can be calculated from the phase-space density f:

$$\rho \equiv \int_{-\infty}^{\infty} f \, du,$$

$$v \equiv \frac{1}{\rho} \int_{-\infty}^{\infty} uf \, du, \qquad (22)$$

$$\theta \equiv \frac{1}{\rho} \int_{-\infty}^{\infty} (u-v)^2 f \, du.$$

1. Conservation of particles

Integrating the test-particle equation, Eq. (18), over u gives

$$\rho_t + (\rho v)_x = 0, \qquad (23)$$

which is the conservation of particles equation.

2. Conservation of momentum

Multiplying the test-particle equation, Eq. (18), by u and integrating, gives

$$\partial_t \int uf \, du + \partial_x \int u^2 f \, du = 0. \qquad (24)$$

(The term involving a is zero after integration by parts and symmetrization of the integrand.) Using the definitions in Eqs. (22), we then have

$$\partial_t \int uf\,du + \partial_x \int u^2 f\,du = (\rho v)_t + (\rho v^2 + \rho\theta)_x = 0. \tag{25}$$

Using Eq. (23), this momentum equation can be written in a more familiar form as

$$v_t + vv_x = -\rho^{-1}(\rho\theta)_x. \tag{26}$$

The quantity $\rho\theta$ is the analog of the pressure: Its gradient causes accelerations. It is proportional to the product of the temperature and the density, as it is in an ideal gas.

3. Dissipation of energy

The energy of the system is not conserved, but is continually dissipated by collisions. Multiplying the test-particle equation by u^2 and integrating, gives

$$\partial_t \int u^2 f\,du + \partial_x \int u^3 f\,du + 2\int uaf\,du. \tag{27}$$

Symmetrizing the integral on the right-hand side, we can show that the rate of energy dissipation $\mathscr{D}$ is negative:

$$\mathscr{D} \equiv 2\int uaf\,du$$
$$= -q \int \int (u'-u)^2|u'-u|f(u)f(u')du\,du'$$
$$\leqslant 0. \tag{28}$$

Thus the energy of the system decreases with time. Using the momentum and continuity equations, and assuming that f is symmetric about $u=v$, we can write Eq. (27) as

$$\theta_t + v\theta_x = -2\theta v_x + \rho^{-1}\mathscr{D}. \tag{29}$$

The term $-2\theta v_x$ on the right-hand side of this equation represents the heating or cooling by compression or expansion.

4. Galilean invariance

Galilean invariance of the test-particle model can be checked by showing that, if $f(x,u,t)$ is a solution of Eq. (18), then $g(x,u,t) \equiv f(x+ct, u+c, t)$ is also a solution. This can be verified by substitution.

IV. SOLUTIONS OF THE TEST-PARTICLE EQUATION

We now discuss solutions of the test-particle equation, all of which are delta functions in velocity space. The effect of the diffusion term $(Df)_{uu}$ in Eq. (17), which is neglected in the test-particle equation, would be to smear these delta functions out. Since the test-particle equation neglects this diffusive term, it has delta function solutions.

A. Spatially uniform solutions

To understand the grouping of particles along the edges of the distribution in phase space we seek solutions of Eq. (18) with the form

$$f(u,t) = \rho \sum_{i=1}^{n} \alpha_i \delta[u - U_i(t)]. \tag{30}$$

Here, ρ is the density of particles, defined in Eq. (22), which requires $\Sigma_i \alpha_i = 1$. Each term in the sum represents one "stream" of particles. A "stream" is defined to be a group of particles moving at the same velocity. The entire velocity distribution is made up of n streams. Substituting Eq. (30) into the test-particle equation, Eq. (18), gives

$$\sum_{i=1}^{n} \alpha_i \dot{U}_i \delta'(u-U_i) = \sum_{i=1}^{n} \alpha_i a(U_i)\delta'(u-U_i). \tag{31}$$

The $\delta'(u-U_i)$ are independent, and setting the coefficients of each independent term equal gives

$$\dot{U}_i = a(U_i) = q\rho \sum_{j=1}^{n} \alpha_j |U_j - U_i|(U_j - U_i). \tag{32}$$

The t^{-2} cooling law can be recovered with just two streams of equal density and of equal and opposite velocities. Setting $n=2$, $U \equiv U_1 = -U_2$, and $\alpha_1 = \alpha_2 = \frac{1}{2}$, Eq. (32) gives

$$\dot{U} = -2q\rho U^2, \tag{33}$$

which has the solution

$$U = U_0/(1 + 2q\rho t U_0), \tag{34}$$

where U_0 is the value of U at time $t=0$. At large times, with $t \gg (2q\rho U_0)^{-1}$, $U \propto t^{-1}$, giving $U^2 \propto t^{-2}$. The two-stream model is successful at predicting the cooling rate of a one-dimensional granular medium. If the constant U_0 is chosen so that the equation matches the simulation exactly at $t=0$, the theory accurately reproduces the initial transient region as well as the ultimate t^{-2} decay shown in Fig. 6.

We can also use this mode to calculate $N_c(t)$, the number of collisions since the beginning of the simulation. Consider a system where the two streams have velocities $\pm U(t)$ and densities $\rho/2$ at time t. The particles in each stream are separated on average by a distance $2/\rho$ and are moving at $2U$ with respect to particles in the other stream. Thus a given particle has a collision rate $n_c = \rho U(t)$. The cumulative number of collisions for the whole system can be calculated:

$$N_c(t) = \frac{N}{2}\int_0^t n_c(t')dt' = \frac{N}{4q}\ln(1+2q\rho U_0 t) = \frac{N^2}{2L}\tau, \tag{35}$$

where $\tau \equiv \ln(1+2q\rho U_0 t)$ and $L \equiv 2qN$. This result can be expressed in terms of τ_c in Eq. (6) as

$$\tau_c = \tau. \tag{36}$$

Figure 7 compares the prediction in Eq. (36) with the five simulations shown in Figs. 1–6. The data are collapsed onto a straight line as predicted, but the slope is significantly greater than 1. (The least squares fit gives a slope 1.142.) The "collision clock" runs faster than the "two-stream clock." Perhaps this is because the two-stream model neglects the dispersion of the velocity distribution and so ignores collisions between particles within the same
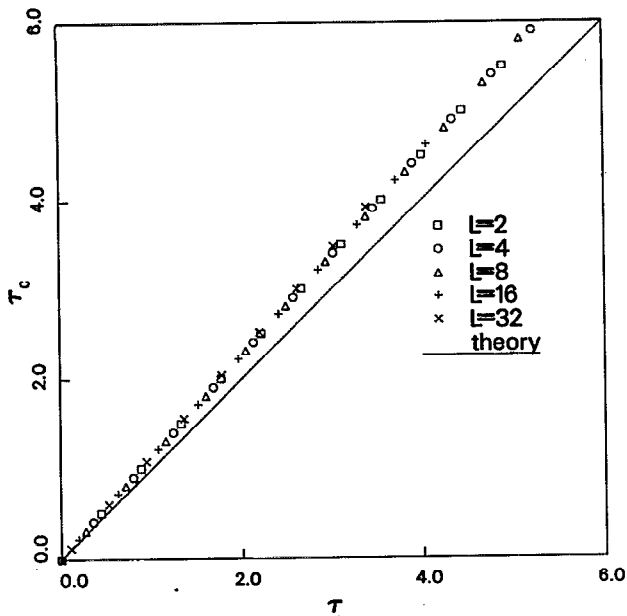
FIG. 7. Number of collisions (measured by $\tau_c \equiv 2LN_c/N^2$) versus time (measured by $\tau \equiv \ln(1+2q\rho_0 t)$) for the simulations of Fig. 5 and 6. The solid line is the relationship predicted by Eqs. (35) and (36)
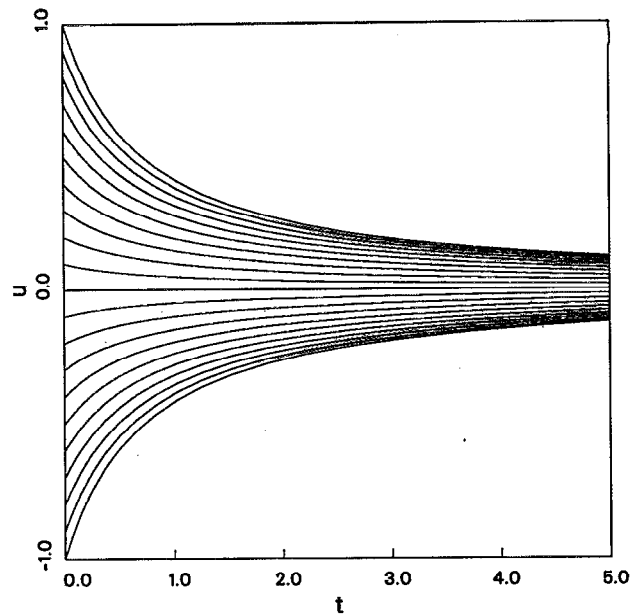

FIG. 8. A solution of the test-particle equation composed of 21 streams of equal strength. Initially, the streams are spaced evenly between $u=1$ and $u=-1$. The streams approach 0 as the gas cools. The streams become concentrated at the edges of the velocity distribution.

stream. But collapsing the data in Fig. 7 onto a straight line is a nontrivial success for this qualitative model. We do not have a quantitative explanation of the slope in Fig. 7.

Studying the system described by Eq. (32) with the $n=5$ case gives insight into the emergence of the bimodal velocity distribution from more general initial conditions. We choose a distribution of five streams symmetric about $u=0$. Set the streams at $u=U_2, U_1, 0, -U_1, -U_2$ with strengths $\alpha_2, \alpha_1, \alpha_0, \alpha_1, \alpha_2$, respectively. Choose $U_2 > U_1$. Then Eq. (32) reduces to

$$(1/q\rho)\dot{U}_1 = -4\alpha_2 U_1 U_2 - (\alpha_0+4\alpha_1)U_1^2,$$

$$(1/q\rho)\dot{U}_2 = -(\alpha_0+2\alpha_1+4\alpha_2)U_2^2-2\alpha_1 U_1^2. \tag{37}$$

Define

$$U_* \equiv U_1/U_2 \tag{38}$$

which is a measure of the shape of the velocity distribution. For $U_* \approx 1$, $U_2 \approx U_1$, and there are two streams at each edge of the velocity distribution. If $U_* \approx 0$, there are three streams at the center of the velocity distribution. Here, $U_2 > U_1$ requires $0 < U_* < 1$. Using Eq. (37), we find that

$$\dot{U}_* = q\rho[(\dot{U}_1 U_2 - U_1\dot{U}_2)/U_2^2]$$

$$= q\rho U_2[\alpha_0 U_*(1-U_*)+2\alpha_1 U_*(1-U_*)^2] > 0. \tag{39}$$

Thus $\dot{U}_* = 0$ for $U_* = 0$ or 1 but $\dot{U}_* > 0$ for $0 < U_* < 1$. Any stream between $u=0$ and $u=U_2$ will migrate toward the edge of the velocity distribution, i.e., toward U_2. This behavior is consistent with Fig. 1.

The tendency for the streams to move toward the edges of the velocity distribution can be demonstrated at larger n. Fig. 8 shows the time evolution of 21 streams of equal

strength. Each U_i moves toward $u=0$ as the gas cools. The streams initially are equally spaced in u, but by time $t=5$ the streams at the edges are much closer to each other than to those in the middle, i.e., the distribution becomes bimodal.

B. Spatially varying solutions: The two stream model

A generalization of the solutions presented in the previous section is

$$f(u,x,t) = \sum_i \rho_i(x,t)\delta[u-U_i(x,t)]. \tag{40}$$

Substitution into the test-particle equation yields a continuity and a momentum equation:

$$\rho_{it}+(U_i\rho_i)_x=0,$$

$$U_{it}+U_iU_{ix}=a(U_i), \tag{41}$$

for each i. The bimodal distribution suggests we may be able to understand the behavior of the system using just two streams. For two streams, we have

$$\rho_{1t}+(U_1\rho_1)_x=0,$$

$$\rho_{2t}+(U_2\rho_2)_x=0,$$

$$U_{1t}+U_1U_{1x}=q\rho_2|U_2-U_1|(U_2-U_1),$$

$$U_{2t}+U_2U_{2x}=q\rho_1|U_2-U_1|(U_1-U_2). \tag{42}$$

This is the "two-stream" model. Despite its simplicity, it successfully predicts the type of instabilities that develop as a uniformly excited medium cools.

We begin by nondimensionalizing the two-stream model in Eq. (42) with

S. McNamara and W. R. Young   41

$$U_i = U_0 \hat{U}_i, \quad \rho_i = \rho_0 \hat{\rho}_i, \quad x = \frac{\hat{x}}{2q\rho_0}, \quad t = \frac{\hat{t}}{2q\rho_0 U_0}, \quad (43)$$

where $i = 1$ or 2, U_0 is the initial root-mean square (rms) velocity and ρ_0 is the average density (with dimensions of particles per length). Here, ρ_0 is also used to define the nondimensional length. One unit of $\hat{x}$ is the distance which, on average, contains $1/2q$ particles. If there are N particles in the domain $0 < x < 1$, then $\rho_0 = 1/N$ and the domain is $0 < \hat{x} < L \equiv 2qN$.

After the scaling in Eq. (43), q is eliminated from the two-stream equations:

$$\hat{\rho}_{1\hat{t}} + (\hat{U}_1 \hat{\rho}_1)_{\hat{x}} = 0,$$

$$\hat{\rho}_{2\hat{t}} + (\hat{U}_2 \hat{\rho}_2)_{\hat{x}} = 0,$$

$$\hat{U}_{1\hat{t}} + \hat{U}_1 \hat{U}_{1\hat{x}} = \hat{\rho}_2 |\hat{U}_2 - \hat{U}_1| (\hat{U}_2 - \hat{U}_1), \quad (44)$$

$$\hat{U}_{2\hat{t}} + \hat{U}_2 \hat{U}_{2\hat{x}} = \hat{\rho}_1 |\hat{U}_2 - \hat{U}_1| (\hat{U}_1 - \hat{U}_2).$$

However, it is essential to realize that $0 < \hat{x} < L$ so that the nondimensional parameter $L = 2qN$ does remain in the formulation, and can be regarded as a nondimensional domain size. This is the only combination of the coefficient of restitution and the number of particles in the two-stream model. Since the condition for inelastic collapse in Eq. (3) involves a different combination, the two-stream model cannot capture this condition, nor predict inelastic collapse.

In dimensionless variables, the spatially uniform solution in Eq. (34) is

$$\hat{\rho}_1 = \hat{\rho}_2 = \tfrac{1}{2}, \quad \hat{U}_1 = -\hat{U}_2 = f(t) \equiv 1/(1 + \hat{t}). \quad (45)$$

We now examine the linear stability of the time-dependent solution in Eq (45). For this analysis, a convenient set of variables is θ_i and v_i, defined by

$$\hat{\rho}_i = \tfrac{1}{2} + f^{-1}\theta_i, \quad \hat{U}_1 = f + v_1, \quad \hat{U}_2 = -f + v_2. \quad (46)$$

We also use

$$\tau \equiv \ln(1 + \hat{t}) \quad (47)$$

as a time variable.

It was shown earlier, in Eqs. (35) and (36), that τ is proportional to the number of collisions. Thus τ is a more natural way to measure time. The rate of evolution is determined by the characteristic velocity of the particles, which changes as the gas cools. Much more happens during a unit of $\hat{t}$ at the beginning of the simulation than a unit of $\hat{t}$ at the end. Using τ to measure time takes the cooling into account so that a unit of τ at the beginning contains the same number of collisions as one at the end.

In terms of the variables in Eqs. (46) and (47), the linearized two-stream equations are

$$\theta_{1\tau} + \theta_1 + \theta_{1\hat{x}} + \tfrac{1}{2}v_{1\hat{x}} = 0,$$

$$\theta_{2\tau} + \theta_2 - \theta_{2\hat{x}} + \tfrac{1}{2}v_{2\hat{x}} = 0,$$

$$v_{1\tau} + v_{1\hat{x}} = -v_1 + v_2 - 2\theta_2, \quad (48)$$

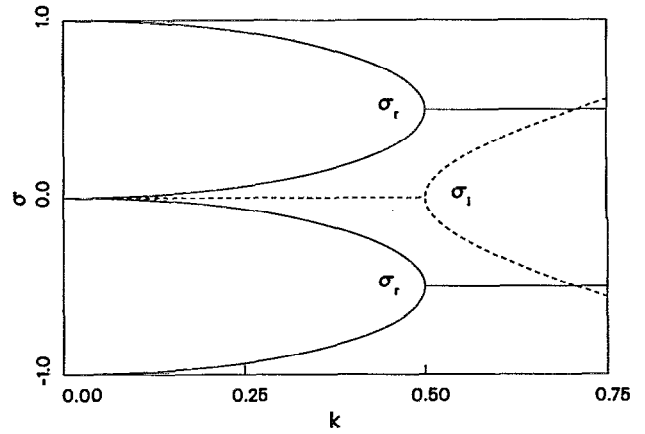$$v_{2\tau} - v_{2\hat{x}} = v_1 - v_2 + 2\theta_1.$$

FIG. 9. Dispersion relation for waves in the two-stream model. The real part is shown with solid lines, dashed lines indicate the imaginary part. There are four values of σ for each value of k.

Since all the coefficients of the dependent variables in Eq. (48) are independent of τ, we use the usual substitution, $\theta_1 = \tilde{\theta}_1 \exp(ik\hat{x} + s\tau)$, $v_1 = \tilde{v}_1 \exp(ik\hat{x} + s\tau)$, to obtain a dispersion relation

$$\sigma/(\sigma^2 + k^2) = (\sigma^2 + k^2)/\sigma, \quad (49)$$

where $\sigma \equiv s + 1$. The dispersion relation above can be further simplified to

$$\sigma = \tfrac{1}{2}(\pm 1 \pm \sqrt{1 - 4k^2}), \quad (50)$$

where the four different combinations of $+$ and $-$ generate four branches. Thus, the linearized two-stream model has four modes corresponding to the four time derivatives in Eq. (42).

The condition for instability needs to be carefully computed, since the "time" τ is not linearly related to $\hat{t}$. We have

$$v = \tilde{v} \exp(ik\hat{x} + s\tau) = \tilde{v}(1 + \hat{t})^s \exp(ik\hat{x}), \quad (51)$$

so that the velocity perturbation grows for $s > 0$. However, the background velocity is decaying as $(1 + \hat{t})^{-1}$. A stable perturbation must decay at a faster rate, otherwise it will be growing relative to the background velocity. Therefore the condition for instability is $s > -1$ or $\sigma > 0$. A similar result holds for density perturbations:

$$\rho = \tfrac{1}{2} + f^{-1}\theta$$

$$= \tfrac{1}{2} + (1 + \hat{t})\tilde{\theta} \exp(ikx + s\tau)$$

$$= \tfrac{1}{2} + \tilde{\theta} \exp(ikx)(1 + \hat{t})^{s+1}. \quad (52)$$

From this equation, it can be seen that density perturbations grow if $s + 1 = \sigma > 0$.

Figure 9 shows the dispersion relation, Eq. (49). For $\hat{k} < 1/2$, there are two unstable, growing modes and two stable, decaying modes. The growth rate σ is purely real so these stationary long waves grow without propagating. For $\hat{k} > 1/2$, σ becomes complex, with Re $\sigma = \pm 1/2$. Because the growth rate has an imaginary part, these short waves are traveling disturbances. However, they also grow or de-

cay, depending on the sign of Re σ. This is an important difference between the present instability calculation and that of Ref. 8, where it was found that sufficiently short waves are stable. Here, the growth rate is smaller for short waves, but still indicates instability.

C. Comparison of the two-stream model with simulations

The two-stream model provides a prediction of the shape of the disturbances. Once the dispersion relation is known, Eq. (48) can be used to find relationships between v_1 and v_2. For the growing modes, we have simply $v_1 = v_2$ so that the two streams move in phase and the mode is "sinuous." (The decaying modes are "varicose" with $v_1 = -v_2$.) The instabilities that arise are indeed of the type predicted by the two-stream model. Examining Figs. 1–4 shows that the streams are always nearly parallel to each other.

The parameter L is the nondimensional length of the domain. It plays a crucial role in determining the behavior of a simulation. As L decreases, the length of the waves that can fit into the domain $0 < \hat{x} < L$ also decreases. If L is too small, then stationary waves, with Im $\sigma = 0$, no longer fit in the domain. If the domain is small, only traveling waves will be present. This qualitative prediction is verified by the simulations of Sec. II. Figure 1 has $L = 2$, and only traveling disturbances are seen. (The oscillation is a superposition of two oppositely directed traveling waves.)

The theory predicts that small-scale traveling disturbances can always exist, but that their growth rate is always less than that of the large-scale stationary disturbances. Thus, in the initial development of the instabilities where linear dynamics is valid, both stationary and traveling disturbances are superimposed but the stationary ones will grow faster. In Fig. 3, where $L = 8$, the unstable mode does not oscillate. We claim that this is because the low wave-number modes in the initial conditions have amplified faster than the high wave-number modes. The trend toward higher harmonics at higher values of L, shown in Fig. 4, is also consistent with the theory. As L increases, long, rapidly growing and nonpropagating disturbances contribute to the distortion of the phase-space density. Figure 5 shows a difference between large and small L suggestive of a transition from stationary to traveling disturbances. The sinuousity ξ can be used to measure the amplitude of the instability:

$$\xi \approx v_1/f \approx v_2/f. \qquad (53)$$

In the large-L simulations, $\xi \approx v/f$ increases roughly monotonically, and more quickly than in the small-L simulations. The small-L simulations show oscillations in ξ superimposed on a slower upward trend, consistent with disturbances that oscillate as well as grow.

A more quantitative comparison of theory and simulation requires knowledge of the boundary conditions at the walls. If the wall reflected the particles elastically, then the velocity of the incoming stream would be equal and opposite to the velocity of the outgoing stream. In our simulations the walls are almost elastic and so the incom-
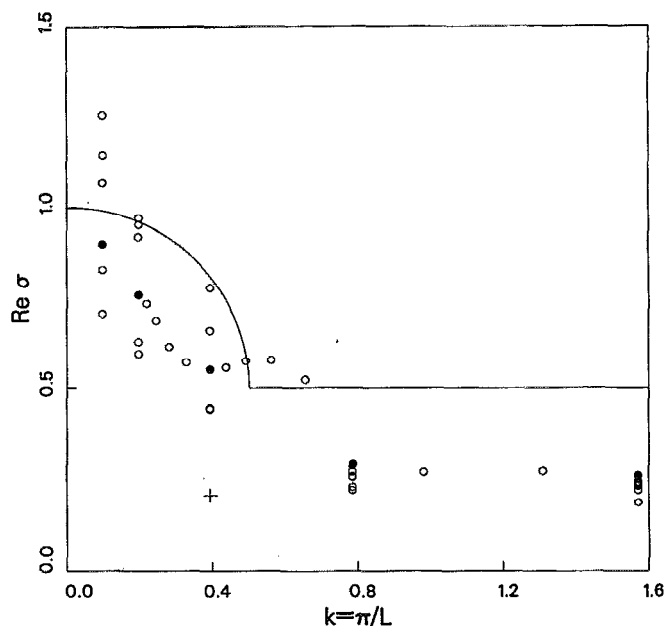

FIG. 10. Comparison of the theoretical (solid line) and simulated (circles) growth rate of instabilities in domains of various sizes. The five solid circles are the five simulations discussed in Figs. 1–6. The solid line is the largest Re σ from the dispersion relation (see Fig. 9). For the data points, the horizontal axis is π/L; for the theoretical curve the horizontal axis is the wave number k. The two are equal if the gravest mode (with a wavelength twice the domain size) is excited in the simulation.

ing stream has a velocity equal and opposite to the outgoing stream with a small difference of order qU. Thus we have $v_1 = -v_2[1 - O(q)]$. This, combined with the requirement $v_1 = v_2$ for growing modes, gives the boundary condition

$$v_1 = 0, \quad v_2 = 0 \quad \text{at} \quad x = 0, L. \qquad (54)$$

This quantizes the waves within the domain and explains why the vibration in Fig. 1 has zero amplitude at the walls. The longest wave that fits in the domain has a wavelength of $2L$. Such a wave is shown in Fig. 3 ($L = 8$). Its wave number is $k = \pi/8$, and it is a stationary, growing disturbance. The next lowest wave that can exist in the box has $k = \pi/4$, and it is too short to be stationary; it is a traveling disturbance and its growth is obscured by that of the lowest mode. In Fig. 4(a) ($L = 16$), both the first and third modes are visible. The theory predicts a change in behavior at $L = 2\pi$. For $L < 2\pi$, the shortest stationary mode no longer fits in the domain and all of the quantizable modes are oscillatory as well as unstable with a growth rate that is independent of wave number [from Eq. (50), Re $\sigma = 1/2$ if $k > 1/2$]. For $L > 2\pi$, stationary modes, with $k < 1/2$, dominate the initial evolution.

Figure 10 compares Re σ of the fastest growing mode of Fig. 9 with an estimate from simulations, obtained by setting Re σ equal to the slope of ln ξ plotted against τ. The wave number of a simulation is determined by assuming that the growing instability is the gravest mode and so has a wavelength of twice the domain length, i.e., $k = \pi/L$. (In the discussion below, we show this assumption is not al-

ways valid.) The five solid circles in Fig. 10 are the five simulations of Figs. 1–7 with $L=2$, 4, 8, 16, and 32. At each of these values of $k=\pi/L$, we have included five additional estimates of σ from simulations with different initial conditions. We have also filled in the gaps between these five selected values of L with ten additional simulations.

There is qualitative agreement between the theoretical curve and the estimated growth rates. In the traveling wave regime (roughly $k>0.5$), the growth rate is independent of wave number. And in the long wave limit the growth rate approaches 1. Considering the crudeness of both the two-stream model and the method of estimating σ, we think the agreement between the theoretical curve and the data points is acceptable. The transition from traveling to stationary waves is visible as an increase in σ. There are two main differences between the theoretical curve and the data points. First, the growth rate in the traveling wave regime is roughly half as large as the predicted value. Second, the boundary between the traveling wave and the stationary wave regimes seems to occur at $k\approx0.7$, rather than at $k=0.5$ as the theory predicts. In addition, there is significant scatter in the experimental points.

We have no explanation for the difference between theory and simulation in the short wave regime except the simplicity of the two-stream model. The two-stream model ignores all of the particles between the two streams. Incorporating the effects of these particles (in, for example, a "three-stream model") might improve the quantitative agreement between theory and simulation.

The second discrepancy, which is that the boundary between oscillatory and direct growth is at $k\approx0.7$, might be due to the difficulty of separating slow oscillations from steady growth. For instance, in Fig. 5, the sinuousity of the $L=4$ curve undergoes one "bounce" in six units of τ_c, more than half the time it took for it to reach $\xi=0.5$. If the bounce took longer (and it does as $k\to1/2$), the sinuousity could cross $\xi=0.5$ at the crest of the first bounce. This would lead to an overestimate of σ, since the apparent slope of $\ln\xi(\tau)$ would include the oscillatory part of σ as well as the growing part.

The point in Fig. 10 marked with a cross near $k=0.4$, $\sigma=0.2$ is anomalous. Like Fig. 3, this simulation has $L=8$ and is within the stationary wave regime. Yet the estimated growth rate is typical of the traveling wave regime. Further, the sinuousity for this particular simulation oscillates and grows. This simulation is shown in Fig. 11, and the reason for its anomalous behavior is at once clear and consistent with the theory. The random initial conditions have strongly excited the second mode instead of the first mode. Thus the wave in this simulation really has a wave number $k=2\pi/8=\pi/4$ (greater than the critical wave number $k=1/2$) instead of $k=\pi/8$, which is the expected wave number if the initial conditions excited the gravest mode.

This points to an additional difficulty with our crude method of estimating σ from the simulations, viz., the random initial conditions excite a mix of modes. The scatter in the estimates of σ, which is evident in Fig. 10, might result from averaging the growth rates of this random superpo-
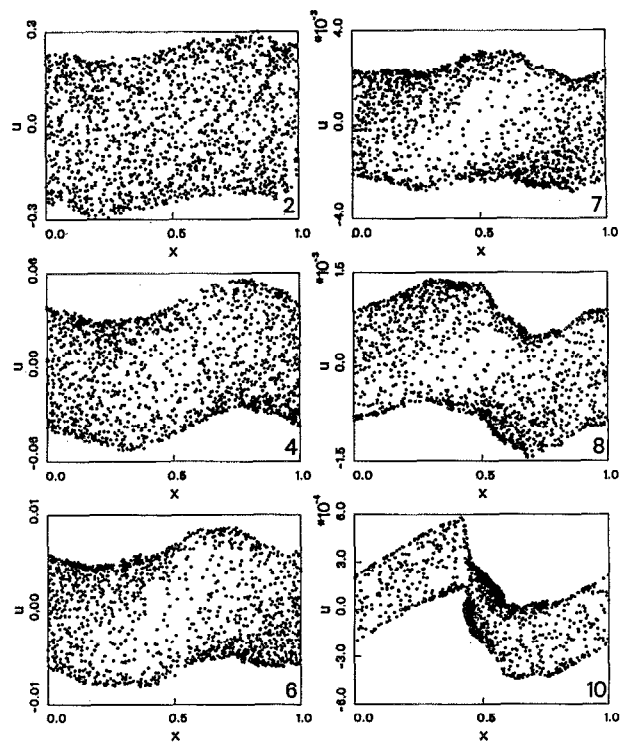

FIG. 11. A simulation at $L=8$, $N=1600$, identical to Fig. 3, except with different initial conditions produced by a random number generator. The numbers in the lower right-hand corner of each panel give the value of τ_c for that panel. Unlike Fig. 3, the dominant disturbance is the second mode. The lowest mode, dominant in Fig. 3, grows without oscillation and has $k=\pi/8<k_c=1/2$, so it only grows, but does not oscillate. The mode here is in the traveling wave regime and has $k=\pi/4>k_c$, and is thus in the traveling wave regime, and oscillates.

sition. This argument rationalizes the observation that the scatter is greater when L is larger. In particular, when $k>1/2$ the theory predicts that all modes have $\mathrm{Re}\,\sigma=0.5$ and so our estimate is not effected if several different modes are superimposed. But in large domains, different modes have different growth rates and different random superpositions (e.g., Fig. 4) will lead to different estimates of $\mathrm{Re}\,\sigma$.

V. CONCLUSIONS

In an attempt to apply a statistical theory to the cooling of a one-dimensional granular medium, the development of strong interparticle correlations was deferred (but not avoided) by taking the double limit in which $N\to\infty$ and $1-r\to0$. This quasielastic limit eliminates the finite time singularities associated with collapse, but simulations show that particle clumps still form throughout the medium (e.g., Fig. 2). The implication is that kinetic theories that neglect interparticle correlations cannot describe the quasielastic system in the long time limit. Instead, the kinetic theory of Sec. III qualitatively captures some of the interesting phenomena that are precursors of the ultimate condensed state (e.g., Fig. 1). These include the rapid development of a bimodal velocity distribution, the growth of

large-scale instabilities and the distinction between stationary and traveling disturbances depending on the domain size.

The two-stream model in Eq. (42) is different from a conventional hydrodynamic model that might be constructed from Eqs. (23), (26), and (29). (For instance, the two-stream model has four linear modes, rather than three.) The exact connection between the two-stream model and conventional hydrodynamics is not clear to us. We emphasize that both the two-stream model and the hydrodynamics in Eqs. (23), (26), and (29) are consequences of the test-particle equation in Eqs. (14) and (18). The two-stream model has the advantage that it is a closed system while the hydrodynamic model requires further elaboration to relate the dissipation term $\mathscr{D}$ in Eq. (29) to ρ, θ, etc.

To summarize, the formation of clumps in an initially uniform one-dimensional granular medium has two stages. First, density inhomogenities grow according to the linear dynamics detailed in this paper. When particle concentrations become high enough, the "molecular chaos" assumption breaks down, and the kinetic theory fails. Second, the inhomogenities become singular in finite time if the threshold for inelastic collapse is exceeded. Otherwise, the clumps grow by merger into a single large clump that persists indefinitely (Fig. 2).

The coefficients of restitution used in our simulations are too close to 1 to be realistic. A carefully polished ball bearing bouncing off a hard, polished metal surface at very low speeds has $r \approx 0.95$ and a "superball" has $r \approx 0.9$, but we have routinely used $r > 0.99$ in this paper. There are two reasons for this restriction. First, large numbers of particles are needed to verify the statistical approach. Second, we have shown that the clustering of particles (the formation of isolated regions of high density, as distinct from inelastic collapse) takes place even up to the highest r used in this paper. The theory indicates that clumping will occur as $r \to 1$, provided that $L = (1 - r)N$ is fixed.

[1] S. McNamara and W. R. Young, "Inelastic collapse and clumping in a one-dimensional granular medium," Phys. Fluids A 4, 496 (1992).

[2] B. Bernu and R. Mazighi, "One-dimensional bounce of inelastically colliding marbles on a wall," J. Phys. A: Math. Gen. 23, 5745 (1990).

[3] G. F. Carnevale, Y. Pomeau, and W. R. Young, "Statistics of ballistic agglomeration," Phys. Rev. Lett. 64, 2913 (1990).

[4] B. E. Sanders and N. L. Ackermann, "Instability in simulated granular chute flow," J. Eng. Mech. 117, 2396 (1991).

[5] M. A. Hopkins and M. Y. Louge, "Inelastic microstructure in rapid granular flows of smooth disks," Phys. Fluids A 3, 47 (1991).

[6] J. T. Jenkins and S. B. Savage, "A theory for the rapid flow of identical, smooth, nearly elastic, spherical particles," J. Fluid Mech. 130, 187 (1983).

[7] P. K. Haff, "Grain flow as a fluid-mechanical phenomenon," J. Fluid Mech. 134, 401 (1983).

[8] M. Babic, "Particle clustering: an instability of rapid granular flows," in Advances in Micromechanics of Granular Materials, edited by H. H. Shen, M. Satake, M. Mehradabi, C. S. Chang, and C. S. Campbell (Elsevier, Amsterdam, 1992), p. 291.

[9] The linear modes of a granular shear flow were also studied by T. M. Mello, P. H. Diamond, and H. Levine, "Hydrodynamic modes of a granular shear flow," Phys. Fluids A 3, 2067 (1991). But in this reference attention is confined to wave vectors that are orthogonal to the velocity. In agreement with Ref. 8, it is found that disturbances with this orientation are stable.

[10] T. G. Drake, "Structural features in granular flows," J. Geophys. Res. 95, NO.B6, 8681 (1990).

[11] D. A. McQuarrie, Statistical Mechanics (Harper & Row, New York, 1976).

[12] Fluctuations ensure that two particles with the same velocity do not experience exacly the same acceleration. The effect of these fluctuations is contained in the term $(Df)_{uu}$ in Eq. (17). The fluctuations in acceleration between different particles moving with the same velocity results in a diffusion in velocity space that is neglected in the test-particle equation.